

Prediction of a potential high-pressure structure of FeSiO₃

R. E. Cohen^{1,2,*} and Yangzheng Lin¹

¹Geophysical Laboratory, Carnegie Institution of Washington, 5251 Broad Branch Road, NW, Washington, DC 20015, USA

²Department of Earth Science, University College London, London WC1E 6BT, United Kingdom

(Received 1 July 2014; revised manuscript received 19 September 2014; published 6 October 2014)

We predict a candidate high-temperature, high-pressure structure of FeSiO₃ with space-group symmetry *Cmmm* by applying an evolutionary algorithm within density functional theory (DFT)+*U* that we call post-perovskite II (PPv-II). An exhaustive search found no other competitive candidate structures with *ABO*₃ composition. We compared the x-ray diffraction pattern of FeSiO₃ PPv-II with experimental results of the recently reported “*H* phase” of (Fe,Mg)SiO₃. The intensities and positions of two main x-ray diffraction peaks of PPv-II FeSiO₃ compare well with those of the *H* phase. We also calculated the static equation of state, the enthalpy, and the bulk modulus of the PPv-II phase and compared it with those of the perovskite (Pv) and post-perovskite (PPv) phases of FeSiO₃. According to the static DFT+*U* computations, the PPv-II phase of FeSiO₃ is less stable than the Pv and PPv phases under lower mantle pressure conditions at *T* = 0 K and has a higher volume. PPv-II may be entropically stabilized, and may be a stable phase in Earth’s lower mantle, coexisting with -PbO₂ (columbite-structure) silica and perovskite, or with magnesiowustite and/or ferropericlaase, depending on the bulk composition.

DOI: 10.1103/PhysRevB.90.140102

PACS number(s): 91.60.-x, 61.50.Ah

In 1987, Knittle and Jeanloz reported that silicate perovskite was stable throughout the Earth’s lower mantle [1], and for a long time it was believed to be the last major phase change in the Earth’s mantle. Ten years ago, the post-perovskite phase was discovered, which explained many features of the Earth’s *D*’ layer at the base of the mantle, and has since been widely believed to be the last mantle phase transition [2]. Recently, a new phase has been reported that was formed by disproportionation of (Mg,Fe)SiO₃ perovskite [3].

We have used the evolutionary algorithm encoded using XTALOPT [4,5] with the QUANTUM ESPRESSO PWSCF code [6,7] and the Perdew-Burke-Ernzerhof (PBE) version of generalized gradient approximation (GGA) for DFT+*U* [GGA+*U*] by searching for the lowest enthalpy phases of FeSiO₃ at 100 GPa with 10, 15, 20, and 30 atoms/primitive cell. The reported cell parameters for the *H* phase were used at initial guess, and each structure was optimized at a constant pressure of 100 GPa.

After calculations for several thousand FeSiO₃ structures, we selected some with the lowest enthalpies for further studies. The symmetry of a selected structure was refined by FINDSYM [8,9] with a tolerance no higher than 0.01. After careful study on the selected structures, we obtained three phases of FeSiO₃ that have the lowest enthalpies at 100 GPa. Perovskite (Pv) and post-perovskite (PPv) are two among the three. The other low enthalpy phase is referred to here as post-perovskite II (PPv-II).

The PPv-II structure is *C*-centered orthorhombic, with a pseudo-hexagonal primitive cell [Figs. 1(a) and 1(c), Table I]. This structure consists of silicon layers stacking along the *a* direction and intercalated Fe ions, which is the same as in the structure of post-perovskite FeSiO₃. In the silicon layer of post-perovskite FeSiO₃, one line of silicon atoms and one line of Fe atoms move about half of its lattice constant along the *a* direction (corresponding to the *c* direction in the

structure of PPv-II) to form post-perovskite II. Accompanying the movement of silicon and Fe lines, some oxygen atoms become bonded to three silicon atoms, while other oxygen atoms become bonded only to one silicon atom (Fig. 1). PPv-II

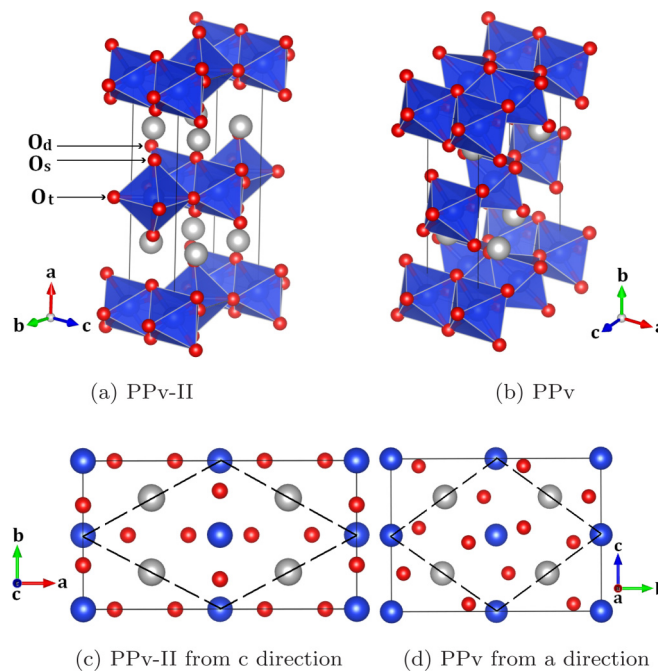


FIG. 1. (Color online) The atomic structure of FeSiO₃ post-perovskite II phase (a) and comparison with post-perovskite FeSiO₃ (b) in one unit cell. (c) View of PPv-II from the *c* direction, (d) View of PPv from the *a* direction. The gray, blue and red spheres represent Fe, Si and O atoms, respectively. The octahedra represent Si with sixfold oxygen coordination. In PPv-II, there are three kinds of O atoms that are in different sharing situations. O_s only bonds to one silicon atom, O_a bonds to two silicon atoms, and O_t is shared by three silicon atoms in the crystal, while all oxygen atoms in PPv are shared by two silicon atoms.

*rcohen@carnegiescience.edu

TABLE I. Structural information of the PPv-II and PPv phases of FeSiO₃ at 100 GPa from GGA+*U*.

| Phase | PPv-II | | | PPv | | | | |
|---------------------------|----------------------|---------------|----------------|---------------------------------|--------------------|----------------|----------|----------|
| Crystal system | Orthorhombic | | | Orthorhombic | | | | |
| Space group | <i>Cmmm</i> (No. 65) | | | <i>Cmcm</i> (No. 63) | | | | |
| Cell parameters | <i>a</i> (Å) | <i>b</i> (Å) | <i>c</i> (Å) | <i>a</i> (Å) | <i>b</i> (Å) | <i>c</i> (Å) | | |
| | 10.082 | 5.478 | 2.495 | 2.508 | 8.614 | 6.283 | | |
| | α (deg) | β (deg) | γ (deg) | α (deg) | β (deg) | γ (deg) | | |
| | 90 | 90 | 90 | 90 | 90 | 90 | | |
| Atomic coordinates | Label ^a | <i>x</i> | <i>y</i> | <i>z</i> | Label ^a | <i>x</i> | <i>y</i> | <i>z</i> |
| Fe | 4 <i>e</i> | 0.25 | 0.25 | 0 | 4 <i>c</i> | 0 | 0.743 | 0.25 |
| Si1 | 2 <i>a</i> | 0 | 0 | 0 | 4 <i>a</i> | 0 | 0 | 0 |
| Si2 | 2 <i>c</i> | 0.5 | 0 | 0.5 | | | | |
| O1 | 4 <i>i</i> | 0 | 0.702 | 0 | 4 <i>c</i> | 0 | 0.058 | 0.25 |
| O2 | 4 <i>h</i> | 0.336 | 0 | 0.5 | 8 <i>f</i> | 0 | 0.368 | 0.048 |
| O3 | 4 <i>h</i> | 0.115 | 0 | 0.5 | | | | |
| Interatomic distances (Å) | | | | | | | | |
| Si1-O | 1.630(×2), 1.705(×4) | | | 1.648(×2), 1.718(×4) | | | | |
| Si2-O | 1.652(×2), 1.669(×4) | | | | | | | |
| Average Si-O | 1.672 | | | 1.695 | | | | |
| Fe-O | 2.042(×4), 2.297(×4) | | | 2.030(×2), 2.083(×4), 2.107(×2) | | | | |
| Average Fe-O | 2.170 | | | 2.076 | | | | |

^aThe label letters are Wyckoff labels and the number before each letter is the corresponding multiplicity.

resembles PPv compressed along the silicon surfaces and also along the Fe surfaces while it is pulled in the vertical direction, which is demonstrated by the lattice lengths in Table I. In PPv-II, the average Si-O bond distance is smaller than that of PPv, while the average Fe-O bond distance is larger (Table I).

We calculated the x-ray diffraction patterns of PPv FeSiO₃, PPv-II FeSiO₃, and Pv MgSiO₃ under experimental pressures and wavelengths (Fig. 2). According to Ref. [3], the experimental powder is composed mainly of Pv MgSiO₃ and *H* phase in Fig. 2(a), and the experimental powder is nearly pure *H* phase in Fig. 2(b). *H*110 and *H*101 are the two main peaks of the *H* phase based on these experimental XRD patterns. Surprisingly, PPv-II FeSiO₃ also has two main peaks 400 and 220 whose positions are very close to the peak positions of *H*110 and *H*101 (Fig. 2) despite the lattice lengths of the pseudo-hexagonal primitive cell of PPv-II being different from those of the hexagonal *H* phase in Ref. [3] (Table II).

Note that the experimental intensities are not likely to be reliable as they come from the averaged diffraction of small single crystallites (i.e., diffraction spots rather than rings). The differences in the peak positions of PPv-II from experiment are caused by the difference in composition—ours is for pure FeSiO₃, whereas the experimental pattern contains some Mg. Note that PPv also has two peaks at the peak positions of

*H*110 and *H*101. Zhang *et al.* claim that PPv is ruled out by their data: “In addition to Pv, another set of peaks not corresponding to any previously known phases appeared with particularly conspicuous peaks at 2.55 and 2.40 Å (marked *H*110 and *H*101, respectively). These two peaks are close to the diagnostic PPv peaks near 2.5 and 2.4 Å (PPv 022 and 110, respectively), but the high-quality XRD pattern clearly rejects the possibility of PPv” [3]. The best diagnostic peak for PPv-II would be the large *d*-spacing 200 peak, but this weak small 2θ peak may be difficult to observe.

We studied the equations of state (EOS) of the Pv, PPv, and PPv-II phases of FeSiO₃ based on DFT+*U* static calculations. All of our calculations used projector augmented-wave (PAWs) generated with the Perdew-Burke-Ernzerhof (PBE) exchange-correlation functional in the QUANTUM ESPRESSO library for Fe, Si, and O atoms. We used 20-atom cells, $4 \times 4 \times 4$ *k*-point mesh, and 80 Ry cutoff energy for all Pv, PPv, and PPv-II crystals so that the enthalpy difference between FeSiO₃ phases converged within 0.01 eV/FeSiO₃. We used *U* = 6.0, which is the same value as used in the structure searchings. All the phases of FeSiO₃ are in high-spin antiferromagnetic states in

TABLE II. A comparison of the lattice parameters between the primitive cell of PPv-II and the *H* phase in Ref. [3] at 100 GPa.

| | <i>a</i> (Å) | <i>b</i> (Å) | <i>c</i> (Å) | α (deg) | β (deg) | γ (deg) |
|-----------------------|--------------|--------------|--------------|----------------|---------------|----------------|
| <i>H</i> phase [3] | 5.096 | 5.096 | 2.862 | 90 | 90 | 120 |
| PPv-II primitive cell | 5.737 | 5.737 | 2.495 | 90 | 90 | 122.96 |

TABLE III. Parameters of the Vinet equation of state fitted to the GGA+*U* static total energy (*V* is the volume, *K* is the bulk modulus, $K' = dK/dP$, where *P* is pressure, and the subscripts 0 and 100 indicate the values at 0 and 100 GPa, respectively).

| | <i>V</i> ₀ (<i>V</i> ₁₀₀ , Å ³ /FeSiO ₃) | <i>K</i> ₀ (<i>K</i> ₁₀₀ , GPa) | <i>K</i> ' ₀ (<i>K</i> ' ₁₀₀) |
|--------|--|--|---|
| Pv | 44.31 (34.27) | 225 (597) | 4.42 (3.34) |
| PPv | 44.90 (33.98) | 189 (579) | 4.73 (3.47) |
| PPv-II | 45.45 (34.49) | 195 (580) | 4.67 (3.44) |

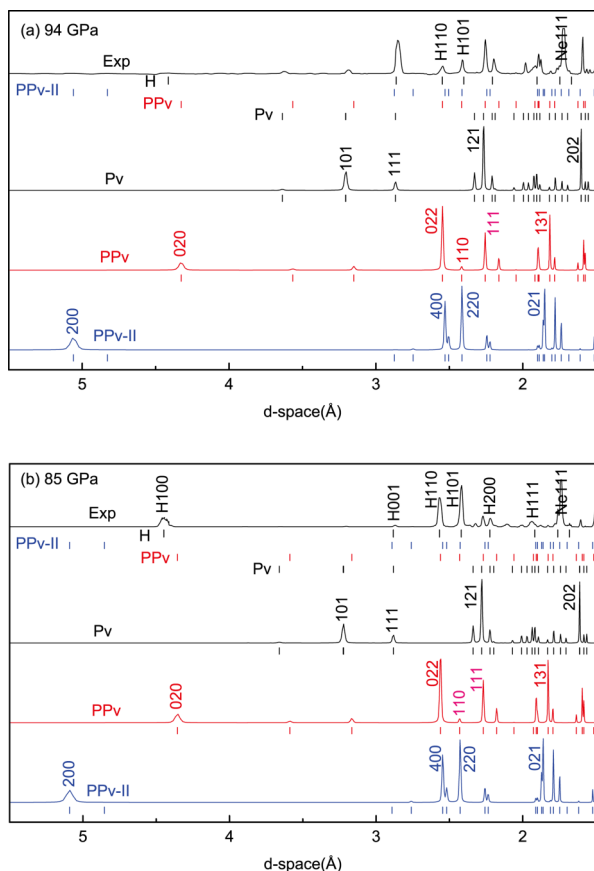


FIG. 2. (Color online) Calculated x-ray diffraction patterns of perovskite (Pv) MgSiO_3 , post-perovskite (PPv) FeSiO_3 , and post-perovskite II (PPv-II) FeSiO_3 crystals at 94 and 85 GPa and their comparisons with experiments. The experimental pattern was read from (a) Fig. 1(c) in Ref. [3] and (b) Fig. 4(a) in Ref. [3]. Here, the horizontal axis indicates d space instead of 2θ in the original figures.

our calculations for they have a lower total energy than the corresponding ferromagnetic and low-spin states.

For each phase of FeSiO_3 , we calculated the static total energies at eight volumes (Fig. 3). The eight volumes

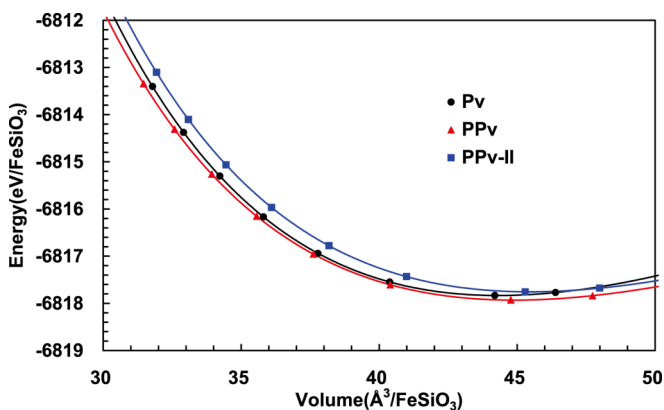


FIG. 3. (Color online) Static energies of FeSiO_3 Pv, PPv, and PPv-II phases using GGA+ U . The solid curves were fitted using the Vinet equation of state [10,11].

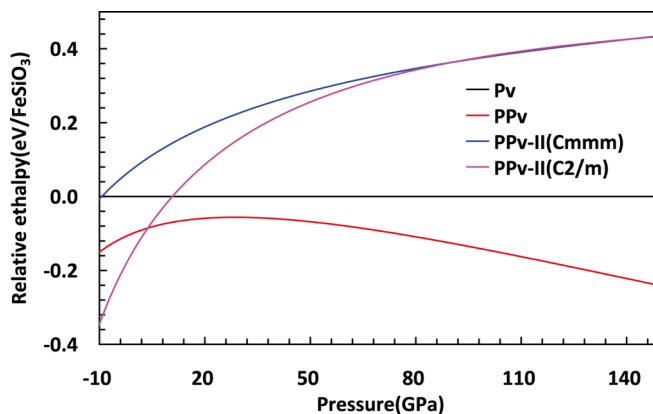


FIG. 4. (Color online) The relative enthalpy of the Pv, PPv, and PPv-II phases of FeSiO_3 from GGA+ U (the enthalpy of Pv FeSiO_3 is zero as the reference).

correspond to eight pressures of $-10, 0, 25, 50, 75, 100, 125,$ and 150 GPa. The EOS parameters were fitted to the $E(V)$ data with a Vinet equation of state [10,11]. At 100 GPa, the bulk modulus of PPv-II is smaller than those of Pv and PPv and the one formula volume of PPv-II is larger (Table III).

The Pv and PPv phases of FeSiO_3 are more stable than the PPv-II phase at high pressures in the lower mantle (Fig. 4). We find that the orthorhombic structure ($Cmmm$) of PPv-II is unstable at low pressure and it has a displacive phase transition to monoclinic symmetry ($C2/m$) (Fig. 4). The monoclinic structure of the PPv-II phase of FeSiO_3 is more stable than Pv at pressures lower than 10.8 GPa and more stable than PPv at 4.5 GPa.

It is intriguing to consider more complex phases that have a mixture or superlattice of PPv Si-O chains and PPv-II Si-O chains. These could either form as a stable structure, or could be due to kinetically hindered solid-state reactions. It also seems possible that the Fe atoms could move in their planes at high temperatures, as in host-guest structures [12].

We have discovered a post-perovskite II phase of FeSiO_3 using crystal structure searches based on enthalpy from DFT calculations at 100 GPa. The crystal of PPv-II is orthorhombic. The structure of PPv-II can be formed from PPv by moving the interval lines of silicon and iron atoms half the lattice constant along their surfaces. Based on the enthalpy from the Vinet equation of state regressed from static total energies of eight volumes, the PPv-II phase of FeSiO_3 is less stable than its Pv and PPv phases at lower mantle pressure conditions. PPv-II has a slightly larger volume than Pv and PPv, and high temperature is probably more propitious to PPv-II than Pv and PPv. Two main peaks in the XRD pattern of PPv-II are in good agreement with the experimental peaks of the H phase both in their positions and relative intensities.

This work is supported by National Science Foundation Grants No. DMS-1025370 and No. EAR-1214807. R.E.C. was supported by the Carnegie Institution and by the European Research Council Advanced Grant ToMcAt. We thank Li Zhang for helpful discussions. We thank Jane Robb for help with the manuscript.

- [1] E. Knittle and R. Jeanloz, *Science* **235**, 668 (1987).
- [2] K. Hirose, J. Brodholt, T. Lay, and D. A. Yuen, *Geophys. Monogr. Ser.* **174**, 1 (2007).
- [3] L. Zhang, Y. Meng, W. Yang, L. Wang, W. L. Mao, Q.-S. Zeng, J. S. Jeong, A. J. Wagner, K. A. Mkhoyan, W. Liu, R. Xu, and H.-k. Mao, *Science* **344**, 877 (2014).
- [4] D. C. Lonie and E. Zurek, *Comput. Phys. Commun.* **182**, 372 (2011).
- [5] “Evolutionary crystal structure prediction”, <http://xtalopt.openmolecules.net/> (2014).
- [6] P. Giannozzi, S. Baroni, N. Bonini, M. Calandra, R. Car, C. Cavazzoni, D. Ceresoli, G. L. Chiarotti, M. Cococcioni, I. Dabo, A. Dal Corso, S. de Gironcoli, S. Fabris, G. Fratesi, R. Gebauer, U. Gerstmann, C. Gougoussis, A. Kokalj, M. Lazzeri, L. Martin-Samos, N. Marzari, F. Mauri, R. Mazzarello, S. Paolini, A. Pasquarello, L. Paulatto, C. Sbraccia, S. Scandolo, G. Sclauzero, A. P. Seitsonen, A. Smogunov, P. Umari, and R. M. Wentzcovitch, *J. Phys.: Condens. Matter* **21**, 395502 (2009).
- [7] “QUANTUM ESPRESSO”, <http://www.quantum-espresso.org> (2014).
- [8] H. T. Stokes and D. M. Hatch, *J. Appl. Crystallogr.* **38**, 237 (2005).
- [9] “Isotropy software suite (Brigham Young University)”, <http://stokes.byu.edu/iso/isotropy.php> (2014).
- [10] P. Vinet, J. Ferrante, J. H. Rose, and J. R. Smith, *J. Geophys. Res.* **92**, 9319 (1987).
- [11] R. E. Cohen, O. Gülseren, and R. J. Hemley, *Am. Mineral.* **85**, 338 (2000).
- [12] O. Degtyareva, V. V. Struzhkin, and R. J. Hemley, *Solid State Commun.* **141**, 164 (2007).